

Research Article

Juan Román-Roche, Álvaro Gómez-León, Fernando Luis and David Zueco*

Bound polariton states in the Dicke-Ising model

https://doi.org/10.1515/nanoph-2024-0568 Received October 24, 2024; accepted January 8, 2025; published online February 17, 2025

Abstract: We present a study of hybrid light—matter excitations in cavity QED materials using the Dicke—Ising model as a theoretical framework. Leveraging linear response theory, we derive the exact excitations of the system in the thermodynamic limit. Our results demonstrate that the cavity can localize spin excitations, leading to the formation of bound polaritons, where the cavity acts as an impurity of the two-excitation band, localizing spin-wave pairs around single-spin domains. We derive the condition for the existence of these bound states and discuss its satisfiability in different regimes. Finally, we show that these effects persist in finite systems using exact-diagonalization calculations.

Keywords: cavity QED materials; bound states; quantum materials

1 Introduction

The control of quantum matter with quantum light is a common pursuit in quantum optics. Initially, the focus was on minimalistic matter such as single atoms and molecules. Due to the weak light—matter coupling, it was realized that photons need to be confined in cavities, giving rise to cavity quantum electrodynamics (cQED) [1], [2]. This field has since evolved to consider more complex forms of matter as well. First, using the cavity as a probe for materials in cavity-enhanced spectroscopy, and more recently, to push the

*Corresponding author: David Zueco, Instituto de Nanociencia y Materiales de Aragón (INMA), CSIC-Universidad de Zaragoza, Zaragoza 50009, Spain; and Departamento de Física de la Materia Condensada, Universidad de Zaragoza, Zaragoza 50009, Spain, E-mail: dzueco@unizar.es. https://orcid.org/0000-0003-4478-1948

Juan Román-Roche and Fernando Luis, Instituto de Nanociencia y Materiales de Aragón (INMA), CSIC-Universidad de Zaragoza, Zaragoza 50009, Spain; and Departamento de Física de la Materia Condensada, Universidad de Zaragoza, Zaragoza 50009, Spain,

E-mail: jroman@unizar.es (J. Román-Roche), fluis@unizar.es (F. Luis). https://orcid.org/0000-0003-2995-6615 (J. Román-Roche). https://orcid.org/0000-0001-6284-0521 (F. Luis)

Álvaro Gómez-León, Institute of Fundamental Physics IFF-CSIC, Calle Serrano 113b, 28006 Madrid, Spain, E-mail: a.gomez.leon@csic.es. https://orcid.org/0000-0002-3990-5259

boundaries of light–matter interaction to explore whether quantum light, either a few photons or vacuum states, can alter the properties of matter [3]–[5]. Seminal experimental demonstrations modifying and controlling conductivity [6], [7], magnetism [8], and the metal-to-insulator transition [9] led to envisioning novel phenomenology emerging from the hybridization of light and matter, such as modifications of chemical reactions [10]–[12], changes in the critical temperature in superconductivity [13], [14], or alterations in magnetism [15], [16], topology [17]–[22], ferroelectricity [23]–[25], and transport in excitonic [26], molecular [27], and disordered electronic systems [28]–[30].

Matter alterations can be underlain by the modification of the ground (thermal) state, and/or from changes to the excitation spectrum. The mixing of two near-resonant energy levels gives rise to polaritons, hybrid states of light and matter that exhibit properties of both constituents [31]. Here, we focus on a key scenario of excitation hybridization: when a continuum couples to a discrete level it can give rise to new discrete levels outside of the continuum, known as bound states. In waveguide QED, the role of the continuum is played by the electromagnetic modes of the waveguide and a coupled emitter provides the discrete energy level. The resulting bound state is spatially localized around the emitter. These bound states have attracted significant attention due to their ability to control light emission, such as inhibiting or enhancing spontaneous emission [32]-[41]. They can also mediate long-range interactions between emitters [42]-[54]. In cavity QED materials, light and matter exchange their roles with respect to waveguide QED, as it is common to consider a macroscopic material that hosts a continuum of energy levels, in the form of bands, coupled to a single cavity mode [17], [55]–[58].

In this paper, we discuss the emergence of bound polaritons in cavity QED materials. These are localized bound states arising from the hybridization of the material energy band with the cavity mode. For this purpose, we employ the Dicke–Ising model, i.e., a spin-1/2 Ising chain coupled transversally to the quantum field fluctuations of the cavity, see Figure 1(a). It generalizes the Dicke model by introducing intrinsic (Ising) interactions among the two-level systems, and it extends the Ising model by considering a quantum transverse field. While it serves as a toy model for a magnetic material coupled to a cavity, it can also be

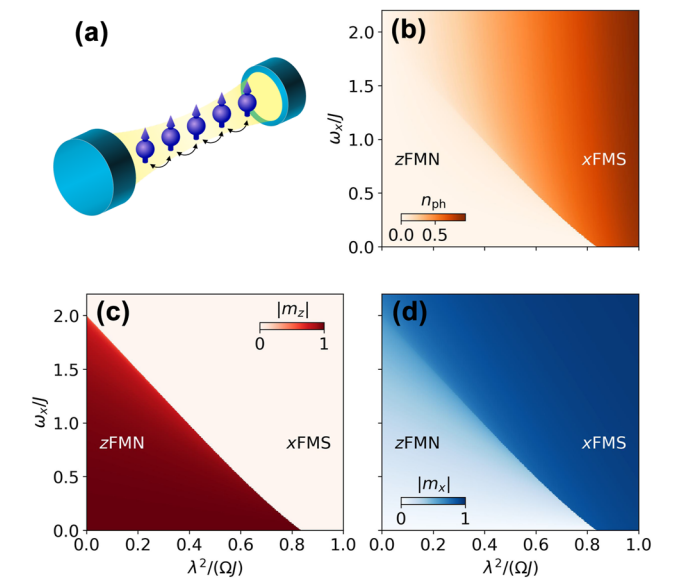


Figure 1: Sketch (a) and phase diagram (b-d) of the Dicke-Ising model in the $(\lambda^2/\Omega, \omega_x)$ plane. (b) Number of photons, $n_{\rm ph}$, which is an order parameter of the x-ferromagnetic superradiant (xFMS) phase for $\omega_x = 0$. (c) Longitudinal magnetization, m_z , which is the order parameter of the z-ferromagnetic normal (zFMN) phase. (d) Transverse magnetization, m_x , which is another order parameter of the xFMS phase for $\omega_x = 0$.

experimentally realized with an array of superconducting gubits coupled to a one-dimensional transmission-line resonator [59]. Crucially, it is exactly solvable in the thermodynamic limit $(N \to \infty)$ with N the number of spins) and its phase diagram is well known [60], [61]. Additionally, using a linear response theory developed by us for cavity QED materials, the excitations can be obtained exactly [62]. This allows us to determine the conditions for the existence of bound polaritons and establish a connection with the bound states in waveguide QED. We show the formation of localized polaritonic bound states hybridizing spin-wave pairs and the cavity photon near the band edges. The reason for this is that the model, through a Jordan-Wigner transformation, can be mapped onto an impurity model, more specifically, a boson localized within the real space of a continuum of fermions.

The rest of the paper is organized as follows. In Section 2, the light-matter model is presented. Section 3 is the main part of our work, where we solve the Dicke-Ising model, including its equilibrium and linear response. Additionally, we prove the existence of bound polariton states. We also perform exact diagonalization calculations for finite systems. Tautologically, we conclude with the conclusions. The microscopic theory of the light-matter Hamiltonian is presented in Appendix A, and the calculation of the dressed material response is presented in appendix B.

2 Model

The light-matter Hamiltonian for a magnetic material coupled to a uniform cavity mode reads

$$H = H_m - \frac{\lambda}{\sqrt{N}} \sum_{i}^{N} \frac{1}{\mu_B} \boldsymbol{m}_j \cdot \boldsymbol{u} (a + a^{\dagger}) + \Omega a^{\dagger} a, \quad (1)$$

with a, a^{\dagger} bosonic annihilation and creation operators, $[a, a^{\dagger}] = 1$, and m_i the magnetic dipole operators of the material (see Appendix A for a derivation). Here, $H_{\rm m}$ is the Hamiltonian of the bare magnetic material and $\lambda/\sqrt{N} =$ $\mu_B B$ is the Zeeman coupling to the magnetic field of the cavity, $\mathbf{B} = B\mathbf{u}$. Importantly, we consider the material in the thermodynamic limit for the number of magnetic dipoles, $N \to \infty$. The cavity field intensity depends on the inverse square root of the mode volume $B \sim 1/\sqrt{V}$. To ensure a well-defined thermodynamic limit, we assume a finite density of dipoles in the cavity, $\rho = N/V = \text{cst.}$ Accordingly, we find that $B \sim 1/\sqrt{N}$ for $N \to \infty$.

We will consider a toy model of a magnetic material, the spin-1/2 Ising chain in transverse field, with transverse coupling to the cavity, such that

$$H_m = \frac{\omega_x}{2} \sum_{j}^{N} \sigma_j^x - J \sum_{j}^{N} \sigma_j^z \sigma_{j+1}^z$$
 (2)

and

$$\frac{1}{\mu_B} \boldsymbol{m}_j \cdot \boldsymbol{u} = \sigma_j^{\boldsymbol{x}}, \tag{3}$$

with σ_j^{α} the Pauli matrices, $\left[\sigma_i^{\alpha},\sigma_j^{\beta}\right]=\delta_{ij}2\epsilon_{\alpha\beta\gamma}\sigma_i^{\gamma}$ and $\epsilon_{\alpha\beta\gamma}$ the Levi-Civita symbol. The full light-matter model is termed the (transverse) Dicke-Ising model [59]-[61], [63]-[66]. For vanishing transverse field, the model has a $\mathbb{Z}_2 \times \mathbb{Z}_2$ symmetry. The first symmetry corresponds to a spin flip, $\sigma_j^z \to -\sigma_j^z$, and in the bare Ising model, it is spontaneously broken in a second-order phase transition from a paramagnetic to a ferromagnetic phase. The second symmetry corresponds to a simultaneous cavity field and spin flip, $a \to -a$ and $\sigma_i^x \to -\sigma_i^x$, and in the bare Dicke model, it is spontaneously broken in a second-order phase transition from a paramagnetic normal to a ferromagnetic superradiant phase. Their combination gives rise to a firstorder phase transition in the Dicke-Ising model between two symmetry-broken phases: an x-ferromagnetic superradiant (xFMS) phase for large g^2/Ω and a z-ferromagnetic normal (zFMN) phase for large J. A nonzero classical transverse field breaks the Dicke symmetry, but the model still features a first-order phase transition between the xFMS phase where the order direction is fixed by the classical field to a symmetry-broken zFMN phase. Alternatively, the Ising chain with longitudinal coupling to the cavity has been studied in Ref. [67]. The model defined by Eqs. (1) and (2) is sketched in Figure 1(a).

3 Exact solution in the thermodynamic limit

Following [62], the equilibrium and linear response properties of model (1) can be computed exactly in the thermodynamic limit, $N \to \infty$. This is essentially because the cavity mediates collective all-to-all interactions between the spins, which can be treated exactly with a mean-field approach.

3.1 Ground state phase diagram

The equilibrium properties are obtained by solving the mean-field effective Hamiltonian [68]

$$H_{\text{eff}}^{\text{MF}} = \frac{\tilde{\omega}_x}{2} \sum_{j}^{N} \sigma_j^x - J \sum_{j}^{N} \sigma_j^z \sigma_{j+1}^z + \frac{N\lambda^2}{\Omega} m_\chi^2, \tag{4}$$

with $\tilde{\omega}_x = \omega_x - 4\lambda^2/\Omega m_x$ and $m_x = N^{-1}\sum_j^N \langle \sigma_j^x \rangle$, variationally with respect to m_x . Then, photonic observables can be computed from the relation $\langle a \rangle = \sqrt{N}\lambda/\Omega m_x$. Equation (4) corresponds to the Ising chain in a transverse field. The transverse field is a combination of the external field and the cavity-induced mean field. It is now clear that adding a longitudinal field would make $H_{\rm eff}^{\rm MF}$ analytically intractable, as the resulting mean-field effective Hamiltonian would correspond to the Ising model with both transverse and longitudinal fields. In the thermodynamic limit, $N \to \infty$, the ground-state energy per spin is given by [69], Chap. 10]

$$\tilde{e}_0(m_x) = \frac{\lambda^2}{\Omega} m_x^2 - \frac{1}{2} \int_{-\pi}^{\pi} \frac{\mathrm{d}k}{2\pi} \tilde{\epsilon}_k, \tag{5}$$

with

$$\tilde{\epsilon}_k = \sqrt{(2J)^2 + \tilde{\omega}_x^2 - 4J\tilde{\omega}_x \cos k}.$$
 (6)

Solving variationally allows us to compute the equilibrium value of m_{χ} numerically and subsequently the longitudinal magnetization as [70]

$$m_{z} = \begin{cases} \left(1 - \left(\frac{\tilde{\omega}_{x}}{2J}\right)^{2}\right)^{\frac{1}{8}} & \text{if } 0 \leq \frac{\tilde{\omega}_{x}}{2J} \leq 1, \\ 0 & \text{if } 1 < \frac{\tilde{\omega}_{x}}{2J}. \end{cases}$$
 (7)

and the number of photons per spin as

$$n_{\rm ph} = \frac{\lambda^2}{\Omega^2} m_{\chi}^2. \tag{8}$$

The zero-temperature phase diagram is presented in Figure 1. The transverse magnetization, m_z , acts as an order parameter for the zFMN phase. For $\omega_x = 0$, the longitudinal magnetization, m_x , and the photon number, $n_{\rm ph}$, act as order parameters for the xFMS phase. An analysis of $e_0(m_x)$ in this case reveals that the system undergoes a first-order phase transition at $\lambda^2/(\Omega I) \approx 0.837$. In the opposite case of vanishing light-matter coupling, $\lambda = 0$, the Ising chain in transverse field is known to undergo a second-order phase transition at $\omega_x/J=2$. In previous solutions of the Dicke-Ising model, the transverse field is set in a direction perpendicular to both the intrinsic interaction and the cavity field, which would be the y direction in our case [60], [61]. Although this difference is subtle, it implies that $m_{\rm v}$ is always an order parameter of the xFMS phase. Then, a Landau analysis of the ground-state energy in terms of its series expansion in powers of m_{ν} reveals the existence of a tricritical point splitting the critical line into a regime of second-order criticality for large ω_x and small λ and a regime of first-order criticality for small ω_x and large λ [61]. In the present case, where the classical transverse field and the cavity fields are aligned, the Landau analysis is not possible. Nevertheless, a visual inspection of the landscape of energy minima of $e_0(m_x)$ reveals the existence of a tricritical point at $\lambda^2/(\Omega I) \approx 0.225$ and $\omega_x/I = 1.427$.

3.2 Linear response theory

The response functions of the hybrid system are given by retarded Green functions [71], Chap. 7]. The retarded Green function for operators *A* and *B* is defined as

$$G_{AB}^{r}(t,t') = -i\theta(t-t')\langle [A(t),B(t')]\rangle. \tag{9}$$

We will be particularly concerned with the photonic propagator

$$D(t) = G_{a,a^{\dagger}}^{r}(t,0), \tag{10}$$

and the matter response function

$$\chi(t) = -\frac{1}{N} G_{C_x, C_x}^r(t, 0), \tag{11}$$

for the coupling operator $C_x = \sum_j^N \sigma_j^x$. In the thermodynamic limit, these are given by

$$D(\omega) = D_0(\omega) - \lambda^2 D_0(\omega) \chi(\omega) D_0(\omega), \tag{12}$$

and

$$\chi(\omega) = \frac{\tilde{\chi}_0(\omega)}{1 + V_{\text{ind}}(\omega)\tilde{\chi}_0(\omega)}$$
(13)

with

$$V_{\text{ind}}(\omega) = \frac{2\lambda^2}{\Omega} \frac{\Omega^2}{(\omega + i0)^2 - \Omega^2},$$
 (14)

Here, D_0 is the bare photonic propagator

$$D_0(\omega) = \frac{1}{\omega + i0 - \Omega},\tag{15}$$

and $\tilde{\chi}_0$ is the matter response function for the mean-field effective matter Hamiltonian of Eq. (4), i.e.,

$$\tilde{\chi}_0(t) = \frac{i}{N} \theta(t) \langle [C_{\chi}(t), C_{\chi}(0)] \rangle_{H_{\text{eff}}^{\text{MF}}}.$$
 (16)

Note that in the cases where $m_{\rm x}=0$, $H_{\rm eff}^{\rm MF}=H_{\rm m}$ and thus $\tilde{\chi}_0 = \chi_0$ is the bare matter response function.

At zero temperature and in the continuum limit, $\tilde{\chi}_0$ is given by (see Appendix B for details)

$$\tilde{\chi}_0(\omega) = -32J^2 \int_{-\pi}^{\pi} \frac{\mathrm{d}k}{2\pi} \frac{\sin^2 k}{\tilde{\epsilon}_k ((\omega + i0)^2 - 4\tilde{\epsilon}_k^2)}.$$
 (17)

Interestingly, we find that $\tilde{\chi}_0$ has poles at $\omega = 2\tilde{\epsilon}_k$. This stems from the fact that the coupling operator, C_x , creates and destroys excitations in pairs of opposite momentum

$$C_{x} = N - 2\sum_{k} \left(\tilde{v}_{k}^{2} + \left(\tilde{u}_{k}^{2} - \tilde{v}_{k}^{2} \right) \tilde{\gamma}_{k}^{\dagger} \tilde{\gamma}_{k} \right.$$
$$\left. + i \tilde{u}_{k} \tilde{v}_{k} \left(\tilde{\gamma}_{k}^{\dagger} \tilde{\gamma}_{-k}^{\dagger} - \tilde{\gamma}_{-k} \tilde{\gamma}_{k} \right) \right), \tag{18}$$

where $\tilde{\gamma}_k$ and $\tilde{\gamma}_k^\dagger$ are the annihilation and creation operators of the Bogoliuvov fermions that constitute the elementary excitations of the effective Ising model (4) after a Jordan-Wigner fermionization [69], Chap. 10]. Here, $\tilde{u}_k =$ $\cos(\tilde{\theta}_k/2)$ and $\tilde{v}_k = \sin(\tilde{\theta}_k/2)$ are the Bogoliubov coefficients, with

$$\tan \tilde{\theta}_k = \frac{\sin k}{\frac{\tilde{\omega}_x}{2J} - \cos k}.$$
 (19)

Thus, χ and D will reflect how the zero-momentum sector of the two-excitation band (a double-energy replica of the single-excitation band) of the Ising model hybridizes with the cavity photon. The fact that excitations are created in pairs of opposite momenta allows one to probe the full band, despite the collective nature of C_x .

This feature brings novel phenomenology that we summarize in Figure 2, where the cavity response (12) is plotted for different scenarios. In all panels, we set $4I = \Omega$, such that the two-excitation band is in resonance with the cavity frequency. Figure 2(a) shows the case of vanishing classical field, $\omega_x = 0$. In this case, the model is nondispersive in the normal phase, as the only source of transverse field is the effective mean field. Instead of a band, the model has a collection of degenerate excitations with energy 21 that

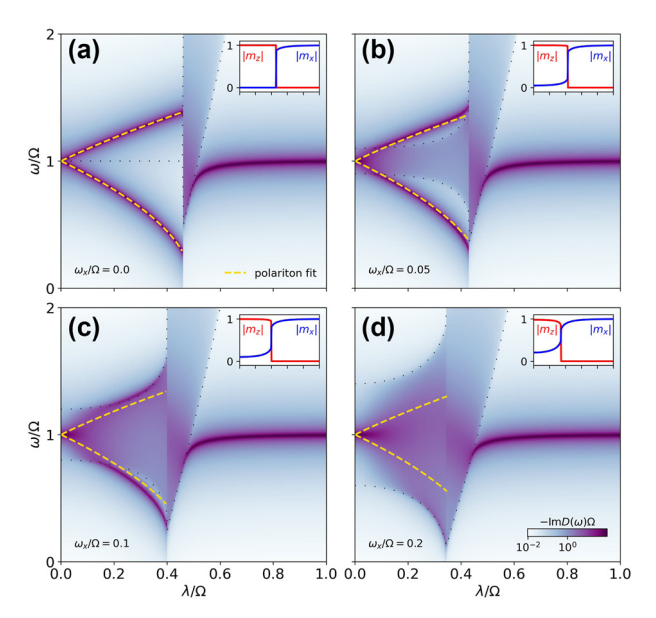


Figure 2: Cavity response, D, of the Dicke model as a function of the collective coupling, λ , for different values of the classical transverse field, $\omega_{\rm x}$. The yellow dashed lines correspond to a fit of the polaritons with a two-oscillator model (see Eq. (20)). The top right insets show the magnetization. The dotted lines mark the edges of the band of the mean-field effective Hamiltonian (4). The Ising interaction is set to $4/ = \Omega$

are linear combinations of domain walls [72]. Accordingly, the zero-momentum sector of the two-excitation band is a degenerate collection of the double excitations that correspond to single-spin flips. This is a typical situation where the cavity is coupled to a collective mode hybridizing with the cavity photon, forming polaritons whose energy can be fitted by a model of two coupled quantum harmonic oscillators of frequencies Ω and 4I:

$$2\Omega_{\pm}^{2} = 4J^{2} + \Omega^{2} \pm \sqrt{\left(4J^{2} - \Omega^{2}\right)^{2} + 32\lambda^{2}J\Omega}.$$
 (20)

At the first-order phase transition, the effective mean field acquires a nonzero value, opening the band. The lower polariton hardens to become the cavity photon in the deep superradiant regime [73].

Figure 2(b)-(d) shows the case of nonzero classical field, $\omega_x \neq 0$. Then, the Ising band (6) is already open in the normal phase and we can understand the model as an impurity model, where the impurity role is played by the cavity.

Before proceeding with the discussion, it is important to distinguish between the two Hamiltonians that we have presented so far, the original Dicke-Ising Hamiltonian defined in Eqs. (1)-(3) and the mean-field effective Hamiltonian of Eg. (4), which is useful for calculations of equilibrium and linear response properties, as we have shown. We have defined Bogoliubov fermions in Eq. (18) as the fermions that diagonalize the mean-field effective Hamiltonian. It is also possible, however, to diagonalize the original Ising model (2) and write the Dicke–Ising model in terms of the corresponding Bogoliubov fermions γ_k and γ_k^\dagger (written without \sim in contrast with those of Eq. (18)). For the following argument, we focus on the full Dicke–Ising Hamiltonian, such that the cavity appears explicitly.

The original collective coupling of the spins to the cavity translates into a momentum-dependent coupling of the Bogoliubov fermions that diagonalize the bare Ising model to the cavity (Cf. Eq. (18)). Furthermore, it is possible to move from a momentum to a real-space representation with a Fourier transform and express \mathcal{C}_x in terms of the domain-wall operators of the bare Ising model

$$C_{x} \propto i \sum_{mn} \eta_{m-n} (\gamma_{m}^{\dagger} \gamma_{n}^{\dagger} - \gamma_{n} \gamma_{m}).$$
 (21)

Here, γ_n^\dagger is a fermionic operator that upon acting on the bare Ising ground state creates a domain wall after the *n*-th spin [72]

$$\gamma_n^{\dagger} = \frac{1}{\sqrt{N}} \sum_k \gamma_k^{\dagger} e^{-ikn}, \qquad (22)$$

and

$$\eta_j = \frac{1}{N} \sum_k \eta_k e^{ikj}, \tag{23}$$

with

$$\eta_k = 2u_k v_k = 2J \sin k/\epsilon_k. \tag{24}$$

In Figure 3, we show that η_j is exponentially localized in real space, with maxima at $j=\pm 1$. Thus, from Eq. (21), we see that the cavity couples maximally to consecutive domain walls $\gamma_m^\dagger \gamma_{m+1}^\dagger$, i.e., to single-spin domains, which is consistent with the fact that $C_x = \sum_j \sigma_j^x$ induces single-spin flips. The coupling to wider domains $\gamma_m^\dagger \gamma_{m+w}^\dagger$ decreases exponentially with the width w of the domain.

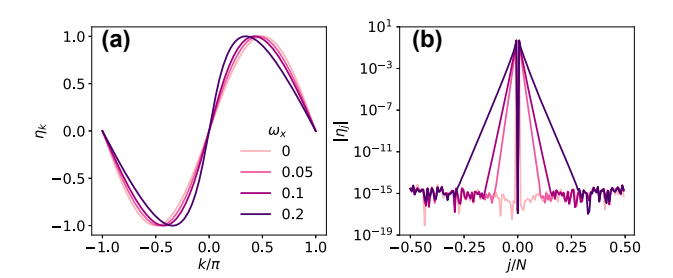


Figure 3: Coupling of the Bogoliubov fermions (a) η_k and (b) its Fourier transform, $\eta_j = \mathcal{F}\{\eta_k\}$, for different values of the classical transverse field, ω_x . The Ising interaction is set to $4J = \Omega$ and the light–matter coupling to $\lambda = 0.2\Omega$. A finite size of N = 150 was used for the Fourier transform.

The spin-boson model in waveguide QED can be described with a spin coupled to a single cavity of a cavity array. The spin acts as an impurity of the cavity array, inducing bound states in which photons are localized around the cavity to which the spin couples. Likewise, in the Dicke–Ising model, the cavity couples only to narrow domains, which are a subset of the two-excitation Ising band. Thus, the cavity acts as an impurity of the two-excitation band, localizing spin-wave pairs around single-spin domains.

This interpretation is further supported by the fact that the equation for the poles of $D(\omega)$ can be shown to be

$$F(\omega) = \omega^2 - \Omega^2 - 4\lambda^2 \Omega \int_{-\pi}^{\pi} \frac{\mathrm{d}k}{2\pi} \tilde{\eta}_k^2 \frac{4\tilde{\epsilon}_k}{\omega^2 - 4\tilde{\epsilon}_k^2} = 0, \quad (25)$$

which can be compared with the equation for the eigenvalues of a discrete system coupled to a continuum with a finite bandwidth [33], in our case the band of the Ising model given by (6). Note that $\tilde{\eta}_k$ and $\tilde{\eta}_j$ present only small quantitative differences with η_k and η_j displayed in Figure 3 in the zFMN phase, where $m_x \ll 1$.

3.3 Existence of bound polariton states

By simple inspection, we observe in Figure 2 that $D(\omega)$ has poles outside the band given by $2\tilde{e}_k$ in Eq. (6). We refer to these states as bound polariton states. While we could simply use the term bound states, we retain the term polaritons since we are within the field of cavity QED materials. Additionally, this highlights their complementarity to the usual bound states in quantum optics, where matter localizes photons around an impurity. Here, it is the cavity that localizes spin excitations.

The possibility of bound states emerging is well known [33], [36], [74]. These states belong to the discrete spectrum and are solutions to $F(\omega)=0$ for ω outside the band. Much is known about bound states, particularly that their existence is primarily determined by the bandwidth, the coupling, and the position of the impurity [44], [54], which in our case is the cavity.

Importantly, in this case, we are able to prove their existence as follows. First, we focus on the possibility of solutions below the lower band edge, given by $2\tilde{\epsilon}_0$, i.e., $F(\omega<2\tilde{\epsilon}_0)=0$. We first assume that $\Omega>2\tilde{\epsilon}_0$, the case depicted in the figure. Thus, the term $\omega^2-\Omega^2<0$, and the integral in (25), is also negative. Therefore, for a solution to exist, the magnitude of the integral must be sufficiently large, which always occurs because the integral diverges as $\omega\to2\tilde{\epsilon}_0$. On the other hand, if $\Omega<2\tilde{\epsilon}_0$, the condition for the existence of bound states is

$$\Omega > 4\lambda^2 \int_{-\pi}^{\pi} \frac{\mathrm{d}k}{2\pi} \frac{\tilde{\eta}_k^2}{\tilde{\epsilon}_k} = 0. \tag{26}$$

Similarly, the argument for bound states above the upper band, in this case $F(\omega > 2\tilde{\epsilon}_{\pi}) = 0$, follows equivalent reasoning, proving, or disproving their existence under the same conditions.

We consider it important to emphasize that these states emerge from a nontrivial system, which, despite being exactly solvable, is a strongly correlated model of matter nonperturbatively coupled to a cavity field. The fact that it can be solved highlights how useful the thermodynamic limit is in cavity QED materials when performing calculations at any value of the light-matter coupling. Similar existence proofs should be obtained in other scenarios, such as intersubband polaritons [56], [75], [76] or lattice fermion models like the SSH model or similar [17], [58]. The existence of bound states in those cases can be discussed following the same procedure as here [75] and should depend on the band limits and the density of states of the matter coupled to the cavity near those band limits.

In Figure 2, we see how tuning the bandwidth with $\omega_{\rm v}$ results in the detachment of bound states from the band edges. Furthermore, we understand their increased visibility (with respect to the band) when they appear, as it is well known that the contribution of the impurity (the cavity) is finite in the bound states. Additionally, the localized nature of bound states explains why the polariton formula (20) accounts well for their energy.

3.4 Finite-size effects

Finally, we present a comparison between our analytical results of Section 3 and finite-size exact-diagonalization results in Figure 4. This allows us to discuss how quickly finite-size effects are washed out as we increase the system size. We compare the analytical results in Figure 4(a), (c) and (e), valid in the thermodynamic limit, with exactdiagonalization results for system sizes up to N = 14 in Figure 4(b), (d), and (f).

Let us begin by comparing Figure 4(a) and (b), which correspond to the case of vanishing classical field. In this case, we observe the formation of polaritons in the normal phase and the opening of the two-excitation band and the hardening of the lower polariton in the superradiant phase in Figure 4(a). The same features are observed in Figure 4(b), although the two-excitation band is not fully formed and instead we can distinguish a collection of discrete levels. Additionally, there are some finite-size effects. Most prominently, there is a pole corresponding to the single-excitation band in the normal phase, at

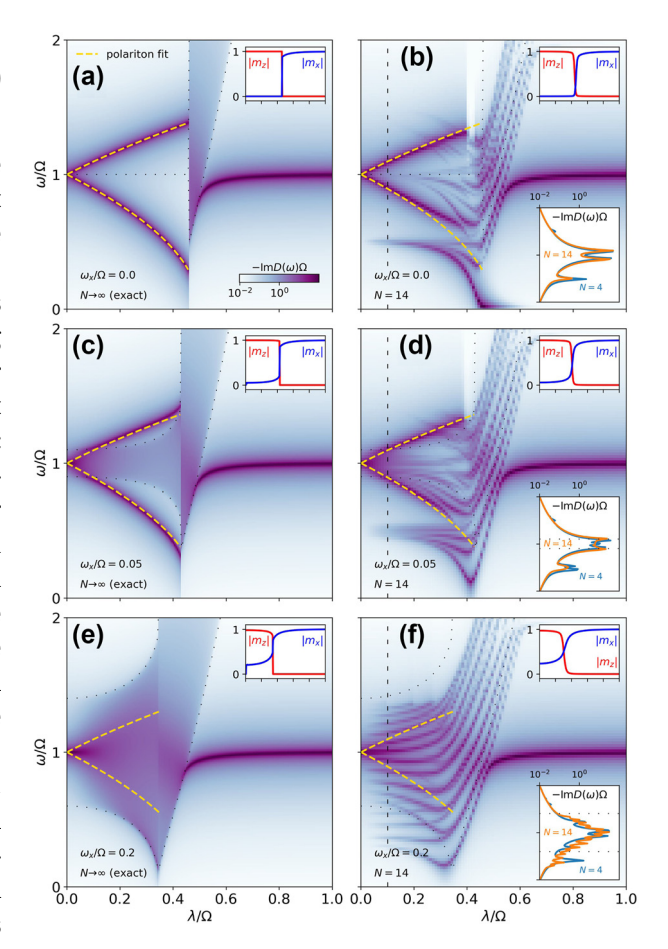


Figure 4: Cavity response, D, of the Dicke-Ising model as a function of the collective coupling, λ , computed analytically in the thermodynamic limit, $N \to \infty$, (left) and with exact diagonalization, N = 14, (right) for different values of the classical field, $\omega_{\rm v}$. The yellow dashed lines correspond to a fit of the polaritons with a two-oscillator model (see Eq. (20)). The top right insets show the magnetizations. The bottom right inset in the right plots shows a vertical cut at the black dashed line for two finite sizes, N = 4 and N = 14. The dotted lines mark the edges of the band of the mean-field effective Hamiltonian (4). The parameters are $\omega_{\rm x}=0$ and $4J=\Omega$. In the exact-diagonalization results, the Fock basis for the photonic Hilbert space is truncated at 40 photons.

 $\omega = 2I = \Omega/2$ for $\lambda \to 0$. This is explained by noting that the coupling operator C_x (18) induces single-spin flips. To understand its effect, it is easier to reason in the limit of small light-matter coupling λ and classical field ω_x . Here, the spins are fully magnetized along z in the ground state $|\uparrow ... \uparrow\rangle$, and the excitations are linear combinations of domain walls of the form $|\uparrow \dots \uparrow \downarrow \dots \downarrow \rangle$. When acting on the ground state, C_x typically creates two contiguous domain walls, i.e., states with single-spin domains of the form $|\uparrow \dots \uparrow\downarrow\uparrow \dots \uparrow\rangle$, which belong to the two-excitation subspace. However, in an open finite chain, C_x also connects the ground state with states of the form $|\uparrow \dots \uparrow\downarrow\rangle$, which present a single domain wall and thus belong to the single-excitation subspace. In the

thermodynamic limit, these edge states represent a vanishing fraction of the single-excitation subspace and thus the visibility of the single excitation band in the photonic propagator becomes negligible as $N \to \infty$. This interpretation is confirmed by the bottom right inset in Figure 4(b), which shows that the intensity of this pole decreases with size, unlike the poles corresponding to the polaritons. Figure 4(c)–(f) features a finite classical field ω_{v} and thus a finite bandwidth in the normal phase. In Figure 4(c), the narrow bandwidth allows the formation of bound polariton states with well-defined energies below and above the band. This is validated in Figure 4(d). Again, we observe additional features that we attribute to finite-size effects. In particular, the single-excitation band, at $\omega = 2I = \Omega/2$ for $\lambda \to 0$. Its visibility is shown to decrease with size in the bottom right inset of Figure 4(d). In Figure 4(e), the large bandwidth prevents the visibility of the bound polariton states. This is confirmed in Figure 4(f) where we observe a collection of closely packed levels of equal visibility that are expected to form the band in the thermodynamic limit. The levels that fall well outside the would-be band are shown to be finite-size artifacts in the bottom right inset of Figure 4(f).

4 Conclusions

In this work, we have studied the emergence of bound polaritons in cavity QED materials using the Dicke–Ising model, whose equilibrium and linear spectrum can be solved exactly in the thermodynamic limit. We demonstrate the existence of bound polariton states, where the cavity-matter coupling leads to the localization of spin waves. These results extend the polariton landscape and present new opportunities to control the dynamics of excitations in quantum materials through cavities.

Our work is based on the large *N* theory for cavity QED materials [62], [77], which yields exact results. To explore how these effects persist in finite systems, we have performed exact-diagonalization calculations. We observe that even in modest system sizes, the described phenomenology is well reproduced, apart from the expected finite-size effects. Finally, we have discussed how the physics described here is generalizable to other cases, such as intersubband polaritons or lattice fermion models like the SSH model coupled to cavities. Additionally, our work extends beyond light—matter systems, including to phonon-polaritons [78] or magnon-spin coupling [79].

Research funding: TED2021-131447B-C21 funded by MCIN/AEI/10.13039/501100011033 and the EU "NextGenerationEU"/PRTR CEX2023-001286-S financed by MICIU/AEI/10.13039/501100011033. The Gobierno de

Aragón (Grant E09-17R Q-MAD), Quantum Spain and the CSIC Quantum Technologies Platform PTI-001. JRR acknowledges support from the Ministry of Universities of the Spanish Government through the grant FPU2020-07231. **Author contributions:** All authors have accepted responsibility for the entire content of this manuscript and approved its submission.

Conflict of interest: Authors state no conflicts of interest. **Data availability:** Data sharing is not applicable to this article as no datasets were generated or analyzed during the current study.

Appendix A: Microscopic theory for magnetic cavity QED

Here, we consider a microscopic derivation of the light—matter Hamiltonian. A complementary perspective can be obtained by employing macroscopic QED theory [80].

For simplicity, we consider a system of N neutral single-electron atoms, each with a nondynamical nucleus with charge e at position \mathbf{R}_j and a dynamical electron with charge -e, bound to the nucleus, at position $\mathbf{R}_j + \mathbf{r}_j$. The derivation can be readily extended to multielectron atoms or molecules. Note that \mathbf{R}_j is a classical variable and \mathbf{r}_j is an operator. The charge density of the system reads

$$\rho(\mathbf{r}) = -e\sum_{j}^{N} \delta^{3}(\mathbf{r} - \mathbf{R}_{j} - \mathbf{r}_{j}) + e\sum_{j}^{N} \delta^{3}(\mathbf{r} - \mathbf{R}_{j}), \quad (A1)$$

and one can define polarization

$$P(\mathbf{r}) = -e\sum_{j}^{N} \mathbf{r}_{j} \int_{0}^{1} \mathrm{d}s \delta^{3}(\mathbf{r} - \mathbf{R}_{j} - s\mathbf{r}_{j})$$
(A2)

and magnetization

$$M(\mathbf{r}) = -e\sum_{j}^{N} \mathbf{r}_{j} \times \dot{\mathbf{r}}_{j} \int_{0}^{1} \mathrm{dss} \delta^{3}(\mathbf{r} - \mathbf{R}_{j} - \mathbf{s}\mathbf{r}_{j})$$
(A3)

fields that satisfy $\nabla \cdot \mathbf{P} = -\rho$ and $\nabla \times \mathbf{M} = \mathbf{j} - \delta_t \mathbf{P}$, with the current density $\mathbf{j}(\mathbf{r}) = -e \sum_{j}^{N} \dot{\mathbf{r}}_{j} \delta^{3}(\mathbf{r} - \mathbf{R}_{j} - \mathbf{r}_{j})$. Here, $\delta^{3}(\mathbf{r})$ is the three-dimensional Dirac delta function.

We start from the Hamiltonian in the Coulomb gauge

$$H = \sum_{j}^{N} \frac{(\boldsymbol{p}_{j} + e\boldsymbol{A}(\boldsymbol{R}_{j} + \boldsymbol{r}_{j}))^{2}}{2m} + V_{C} + V$$
$$+ H_{\text{em}} + \frac{g_{e}\mu_{B}}{2} \sum_{j}^{N} \boldsymbol{\sigma}_{j} \cdot \boldsymbol{B}(\boldsymbol{R}_{j} + \boldsymbol{r}_{j}). \tag{A4}$$

In the Coulomb gauge, the redundancy in the description of the dynamical variables is eliminated by

constraining the vector potential to be transverse, i.e., $\nabla \cdot \mathbf{A} = 0$. The quantized vector potential then reads

$$A(\mathbf{r}) = \sum_{\kappa} A_{\kappa} \mathbf{u}_{\kappa}(\mathbf{r}) a_{\kappa} + \text{h.c.}, \tag{A5}$$

where κ is a four-vector containing the polarization index $\sigma = 1, 2$ and the wavevector \mathbf{k} : $\kappa \equiv \{\mathbf{k}, \sigma\}$. The mode amplitude is $A_k = \sqrt{1/(2\epsilon_0 V \omega_k)}$. The V and ϵ_0 are, respectively, the cavity mode volume and the dielectric constant. We also introduce the bosonic annihilation and creation operators of the κ -th mode: a_{κ} , a_{κ}^{\dagger} , which obey the canonical commutation relations $\left|a_{\kappa},a_{\kappa'}^{\dagger}\right|=\delta_{\kappa\kappa'}$. To maintain as much generality as possible, we have refrained from using a particular spatial dependence for the vector potential. For a specific model, the geometry of the cavity will determine the spatial quantization of the wavevector \mathbf{k} and in turn, the functional form of the mode functions $u_{\kappa}(r)$ [81]. In any case, the following properties hold for the mode functions: $u_{-k}\sigma(r) =$ $u_{k,\sigma}^*(r), u_{k,\sigma}(r) \cdot k = 0, \int_V dV u_{\kappa}^*(r) \cdot u_{\kappa'}(r) = \delta_{\kappa\kappa'}$. Note that in Eq. (A5), the mode functions have been promoted to mode operators, since they depend on the position operator of each particle. By definition, $\mathbf{B} = \nabla \times \mathbf{A}$, so

$$\mathbf{B}(\mathbf{r}) = \sum_{\kappa} B_{\mathbf{k}} \mathbf{u}_{\perp,\kappa}(\mathbf{r}) a_{\kappa} + \text{h.c.}, \tag{A6}$$

where we have defined the transverse mode functions $u_{\perp,\kappa}(r)=|\mathbf{k}|^{-1}\nabla\times u_{\kappa}(r)$ and $B_{\mathbf{k}}=A_{\mathbf{k}}|\mathbf{k}|=A_{\mathbf{k}}\omega_{\mathbf{k}}/c$. Finally, we can express H_{em} as

$$H_{\rm em} = \sum_{\kappa} \omega_{\mathbf{k}} a_{\kappa}^{\dagger} a_{\kappa}. \tag{A7}$$

To move to the multipolar gauge, we will use the Power–Zienau–Woolley (PZW) transformation, defined as

$$U = e^{-i \int d^3 r \mathbf{P}(\mathbf{r}) \cdot \mathbf{A}(\mathbf{r})}.$$
 (A8)

The resulting Hamiltonian in the multipolar gauge reads [82]

$$H = \sum_{j}^{N} \frac{\left(\mathbf{p}_{j} - e\mathbf{r}_{j} \times \int_{0}^{1} \mathrm{dss}\mathbf{B}(\mathbf{R}_{j} + s\mathbf{r}_{j})\right)^{2}}{2m}$$

$$+ V_{C} + V + \sum_{\kappa} \omega_{k} a_{\kappa}^{\dagger} a_{\kappa}$$

$$- i \sum_{\kappa} \omega_{k} A_{k} \int \mathrm{d}^{3} r \mathbf{P}(\mathbf{r}) \cdot \left(\mathbf{u}_{\kappa}(\mathbf{r}) a_{\kappa} - \mathrm{h.c.}\right)$$

$$+ \sum_{\kappa} \omega_{k} \left| A_{k} \int \mathrm{d}^{3} r \mathbf{P}(\mathbf{r}) \cdot \mathbf{u}_{\kappa}(\mathbf{r}) \right|^{2}$$

$$+ \frac{g_{e} \mu_{B}}{2} \sum_{j}^{N} \sigma_{j} \cdot \mathbf{B}(\mathbf{R}_{j} + \mathbf{r}_{j}). \tag{A9}$$

We can now perform the long-wavelength approximation for the electromagnetic field. Instead of taking the crudest approximation, we will perform a multipolar expansion of the polarization and the magnetic field up to the electric quadrupole and magnetic dipole terms. For the polarization, we approximate

$$\delta^{3}(\mathbf{r} - \mathbf{R}_{i} - s\mathbf{r}_{i}) \approx \delta^{3}(\mathbf{r} - \mathbf{R}_{i}) - s(\mathbf{r}_{i}\nabla)\delta^{3}(\mathbf{r} - \mathbf{R}_{i}) \quad (A10)$$

and subsequently

$$\mathbf{P}(\mathbf{r}) = -e\sum_{j}^{N} \mathbf{r}_{j} \delta^{3}(\mathbf{r} - \mathbf{R}_{j}) + \frac{1}{2} e\sum_{j}^{N} \mathbf{r}_{j}(\mathbf{r}_{j} \cdot \nabla) \delta^{3}(\mathbf{r} - \mathbf{R}_{j}).$$
(A11)

With this

$$\int d^{3}r \mathbf{P}(\mathbf{r}) \cdot \mathbf{u}_{\kappa}(\mathbf{r}) = -e \sum_{j}^{N} \mathbf{r}_{j} \cdot \mathbf{u}_{\kappa}(\mathbf{R}_{j})$$

$$+ \frac{1}{2} e \sum_{j}^{N} \mathbf{r}_{j} \cdot \left[(\mathbf{r}_{j} \cdot \nabla) \mathbf{u}_{\kappa}(\mathbf{r}) \right]_{\mathbf{r} = \mathbf{R}_{j}}.$$
(A12)

Similarly, we approximate the magnetic field as $B(R_i + r_i) \approx B(R_i)$. The resulting Hamiltonian reads

$$H = H_{\rm m} - \sum_{j}^{N} \boldsymbol{m}_{j} \cdot \boldsymbol{B}(\boldsymbol{R}_{j}) + \frac{1}{8m} \sum_{j}^{N} \left(\boldsymbol{d}_{j} \times \boldsymbol{B}(\boldsymbol{R}_{j}) \right)^{2}$$

$$+ \sum_{k} \omega_{k} a_{\kappa}^{\dagger} a_{\kappa} - i \sum_{\kappa} \omega_{k} A_{k} \sum_{j}^{N} \boldsymbol{d}_{j} \cdot \left(\boldsymbol{u}_{\kappa}(\boldsymbol{R}_{j}) a_{\kappa} - \text{h.c.} \right)$$

$$+ i \sum_{\kappa} \frac{\omega_{k}^{2}}{c} A_{k} \sum_{j}^{N} \left(\text{Tr}(Q \mathcal{V}_{\kappa}(\boldsymbol{R}_{j}) a_{\kappa} - \text{h.c.} \right)$$

$$+ \sum_{\kappa} \omega_{k} \left| A_{k} \sum_{j}^{N} \boldsymbol{d}_{j} \cdot \boldsymbol{u}_{\kappa}(\boldsymbol{R}_{j}) - A_{k} \frac{\omega_{k}}{c} \sum_{j}^{N} \text{Tr} Q_{j} \mathcal{U}_{\kappa}(\boldsymbol{R}_{j}) \right|^{2},$$
(A13)

with

$$\boldsymbol{d}_{i} = -e\boldsymbol{r}_{i},\tag{A14}$$

$$Q_{j,\alpha\beta} = -\frac{1}{2}e\left(r_{j,\alpha}r_{j,\beta} - \frac{r_j^2}{3}\delta_{\alpha\beta}\right),\tag{A15}$$

$$\boldsymbol{m}_{j} = -\mu_{B} \left(\boldsymbol{r}_{j} \times \boldsymbol{p}_{j} + \frac{g_{e}}{2} \boldsymbol{\sigma}_{j} \right) \tag{A16}$$

the electric dipole, electric quadrupole, and magnetic dipole operators, respectively. To simplify notation, we have defined $U_{\kappa}(\boldsymbol{R}_j) = |\boldsymbol{k}|^{-1} J_{\boldsymbol{u}_{\kappa}}(\boldsymbol{R}_j)$ with $J_{\boldsymbol{u}_{\kappa}}$ the Jacobian matrix of \boldsymbol{u}_{κ} at \boldsymbol{R}_j . This simplified Hamiltonian (A13) reveals the

main forms of atom—light interaction. The second term corresponds to the Zeeman coupling between the total magnetic moment of the electron and the magnetic field. The third term, coupling the electric dipole to the magnetic field, is known as the diamagnetic term. We will disregard it, as it is negligible compared to the others for small per-particle couplings [82]. Note that we could have identified

$$\boldsymbol{E}^{\perp}(\boldsymbol{r}) = -\partial_{t}\boldsymbol{A}(\boldsymbol{r}) = i\sum_{\kappa}\omega_{k}A_{k}(\boldsymbol{u}_{\kappa}(\boldsymbol{r})\boldsymbol{a}_{\kappa} - \text{h.c.}), \quad \text{(A17)}$$

in the fifth and sixth terms, which couple the electric dipole and quadrupole to the transverse electric field, respectively [83]. The last term corresponds to a self-interaction of the polarization field and is typically referred to as the P^2 term. With this, and defining the constants

$$g_k^{\rm m} = \frac{\omega_p}{\sqrt{N}} \sqrt{\frac{\omega_k}{8mc^2}},\tag{A18}$$

$$g_{\mathbf{k}}^{d} = \frac{\omega_{\mathbf{k}}}{\sqrt{N}} \sqrt{\frac{\omega_{p}}{\omega_{\mathbf{k}}}},\tag{A19}$$

$$g_{\mathbf{k}}^{q} = \frac{\omega_{\mathbf{k}}}{\sqrt{N}} \sqrt{\frac{2\omega_{\mathbf{k}}}{mc^{2}}},\tag{A20}$$

we can put together the interaction terms to define electric

$$C_{\kappa}^{e} = -i \sum_{j}^{N} \left(\sqrt{\frac{m\omega_{p}}{2}} \boldsymbol{d}_{j} \cdot \boldsymbol{u}_{\kappa}(\boldsymbol{R}_{j}) - \frac{g_{k}^{q}}{g_{k}^{d}} \frac{m\omega_{p}}{2} \operatorname{Tr}(U_{\kappa}(\boldsymbol{R}_{j})Q_{j}) \right), \tag{A21}$$

and magnetic coupling operators

$$C_{\kappa}^{\mathrm{m}} = -\sum_{j}^{N} \frac{1}{\mu_{B}} \boldsymbol{m}_{j} \cdot \boldsymbol{u}_{\perp,\kappa}(\boldsymbol{R}_{j}), \tag{A22}$$

to finally write the Hamiltonian as

$$H = H_{\rm m} + \sum_{\kappa} \Omega_{\mathbf{k}} a_{\kappa}^{\dagger} a_{\kappa} + \sum_{\kappa} \frac{g_{\mathbf{k}}^{d}}{\Omega_{\mathbf{k}}} |C_{\kappa}^{e}|^{2}$$
$$+ \sum_{\kappa} (g_{\mathbf{k}}^{d} C_{\kappa}^{e} + g_{\mathbf{k}}^{m} C_{\kappa}^{m}) a_{\kappa} + \text{h.c.}, \tag{A23}$$

with $\Omega_{\bf k}=\omega_{\bf k}$. The P^2 term prevents the electronic coupling to the cavity from modifying the ground-state properties with respect to the bare matter model, which already includes electrostatic Coulomb interactions [62], [68], [84]. This is a no-go theorem akin to those derived in the Coulomb gauge from the A^2 term [85]–[90]. The A^2 and P^2 terms ensure gauge invariance in these models [91]–[95]. This motivates the consideration of purely magnetic materials, with negligible polarizability and thus negligible electrostatic dipole–dipole interactions and coupling of the electric dipole to the cavity's electric field [15]. These materials interact with the cavity via the Zeeman coupling of the magnetic

dipole and the cavity's magnetic field. Under these assumptions, and considering for simplicity a single uniform cavity mode, we arrive at Eq. (1).

Appendix B: Computing $\tilde{\chi}_{xx,0}$ for the Ising model

The spectral decomposition of $\tilde{\chi}_{xx,0}$ reads

$$\tilde{\chi}_{xx,0} = -\frac{1}{N} \sum_{n} |\langle n | C_x | 0 \rangle|^2 \frac{2(E_n - E_0)}{\omega_+^2 - (E_n - E_0)^2}, \quad (B1)$$

where $|n\rangle$ is the eigenstate of $H_{\text{eff}}^{\text{MF}}$ (4) with eigenvalue E_n . From Eq. (18), we see that

$$\langle n|C_{x}|0\rangle = \delta_{n0} \left(N + \sum_{k} v_{k}^{2}\right) - 2i \sum_{k} u_{k} v_{k} \langle n|\gamma_{k}^{\dagger} \gamma_{-k}^{\dagger}|0\rangle.$$
(B2)

With this and using Eq. (24), we find

$$\tilde{\chi}_{xx,0} = -\frac{16J^2}{N} \sum_{k} \frac{\sin^2 k}{\epsilon_k (\omega_+^2 - 4\epsilon_k^2)}$$
 (B3)

and in the thermodynamic limit, $\lim_{N\to\infty}N^{-1}\sum_k f_k=\int_{-\pi}^\pi {\rm d}k/(2\pi)f_k$, we obtain Eq. (17).

References

- [1] S. Haroche, "Nobel lecture: controlling photons in a box and exploring the quantum to classical boundary," *Rev. Mod. Phys.*, vol. 85, no. 3, p. 1083, 2013.
- [2] D. J. Wineland, "Nobel lecture: superposition, entanglement, and raising Schrödinger's cat," *Rev. Mod. Phys.*, vol. 85, p. 1103, 2013.
- [3] F. Schlawin, D. M. Kennes, and M. A. Sentef, "Cavity quantum materials," *Appl. Phys. Rev.*, vol. 9, no. 1, p. 011312, 2022.
- [4] F. J. Garcia-Vidal, C. Ciuti, and T. W. Ebbesen, "Manipulating matter by strong coupling to vacuum fields," *Science*, vol. 373, no. 6551, p. eabd0336, 2021.
- [5] J. Bloch, A. Cavalleri, V. Galitski, M. Hafezi, and A. Rubio, "Strongly correlated electron—photon systems," *Nature*, vol. 606, no. 7912, pp. 41—48, 2022.
- [6] G. L. Paravicini-Bagliani, *et al.*, "Magneto-transport controlled by Landau polariton states," *Nat. Phys.*, vol. 15, no. 2, pp. 186—190, 2018.
- [7] F. Appugliese, et al., "Breakdown of topological protection by cavity vacuum fields in the integer quantum hall effect," Science, vol. 375, no. 6584, pp. 1030 – 1034, 2022.
- [8] A. Thomas, et al., "Large enhancement of ferromagnetism under a collective strong coupling of ybco nanoparticles," Nano Lett., vol. 21, no. 10, pp. 4365 – 4370, 2021.
- [9] G. Jarc, et al., "Cavity-mediated thermal control of metal-to-insulator transition in 1t-tas2," *Nature*, vol. 622, no. 7983, pp. 487 – 492, 2023.

- [10] J. Feist, J. Galego, and F. J. Garcia-Vidal, "Polaritonic chemistry with organic molecules," ACS Photonics, vol. 5, no. 1, pp. 205-216, 2017.
- [11] K. Nagarajan, A. Thomas, and T. W. Ebbesen, "Chemistry under vibrational strong coupling," J. Am. Chem. Soc., vol. 143, no. 41, pp. 16877-16889, 2021.
- [12] J. Fregoni, F. J. Garcia-Vidal, and J. Feist, "Theoretical challenges in polaritonic chemistry," ACS Photonics, vol. 9, no. 4, pp. 1096-1107, 2022
- [13] F. Schlawin, A. Cavalleri, and D. Jaksch, "Cavity-mediated electron-photon superconductivity," Phys. Rev. Lett., vol. 122, no. 13, p. 133602, 2019.
- [14] M. A. Sentef, M. Ruggenthaler, and A. Rubio, "Cavity quantumelectrodynamical polaritonically enhanced electron-phonon coupling and its influence on superconductivity," Sci. Adv., vol. 4, no. 11, p. eaau6969, 2018.
- [15] J. Román-Roche, F. Luis, and D. Zueco, "Photon condensation and enhanced magnetism in cavity qed," Phys. Rev. Lett., vol. 127, no. 16, p. 167201, 2021.
- [16] K. Masuki and Y. Ashida, "Cavity moiré materials: controlling magnetic frustration with quantum light-matter interaction," 2024, arXiv:2302.11582 [cond-mat.str-el], https://doi.org/10.1103/ physrevb.109.195173.
- [17] O. Dmytruk and M. Schirò, "Controlling topological phases of matter with quantum light," Commun. Phys., vol. 5, no. 1, p. 271,
- [18] C. A. Downing, T. J. Sturges, G. Weick, M. Stobińska, and L. Martín-Moreno, "Topological phases of polaritons in a cavity waveguide," Phys. Rev. Lett., vol. 123, no. 21, p. 217401, 2019.
- [19] B. Pérez-González, Á. Gómez-León, and G. Platero, "Topology detection in cavity qed," Phys. Chem. Chem. Phys., vol. 24, no. 26, pp. 15860-15870, 2022.
- [20] B. Pérez-González, G. Platero, and Á. Gómez-León, "Light-matter correlations in quantum floquet engineering," 2023, arXiv:2302.12290.
- [21] O. Dmytruk and M. Schirò, "Hybrid light-matter states in topological superconductors coupled to cavity photons," 2023, arXiv:2310.01296 [cond-mat.mes-hall].
- [22] B. Pérez-González, G. Platero, and Á. Gómez-León, "Many-body origin of anomalous floquet phases in cavity-ged materials," 2023, arXiv:2312.10141.
- [23] M. Schuler, D. D. Bernardis, A. M. Läuchli, and P. Rabl, "The vacua of dipolar cavity quantum electrodynamics," SciPost Phys., vol. 9, no. 5, p. 066, 2020.
- [24] Y. Ashida, A. M. C. İmamoğlu, J. Faist, D. Jaksch, A. Cavalleri, and E. Demler, "Quantum electrodynamic control of matter: cavity-enhanced ferroelectric phase transition," Phys. Rev. X, vol. 10, no. 4, p. 041027, 2020.
- [25] D. Shin, et al., "Simulating terahertz field-induced ferroelectricity in quantum paraelectric srtio3," Phys. Rev. Lett., vol. 129, no. 16, p. 167401, 2022.
- [26] J. Feist and F. J. Garcia-Vidal, "Extraordinary exciton conductance induced by strong coupling," Phys. Rev. Lett., vol. 114, no. 19, p. 196402, 2015.
- [27] G. Sandik, J. Feist, F. J. García-Vidal, and T. Schwartz, "Cavity-enhanced energy transport in molecular systems," Nat. Mater., 2024, https://doi.org/10.1038/s41563-024-01962-5.

- [28] C. Ciuti, "Cavity-mediated electron hopping in disordered quantum hall systems," Phys. Rev. B, vol. 104, no. 15, p. 155307, 2021
- [29] G. Arwas and C. Ciuti, "Quantum electron transport controlled by cavity vacuum fields," Phys. Rev. B, vol. 107, no. 4, p. 045425,
- [30] D. Svintsov, G. Alymov, Z. Devizorova, and L. Martin-Moreno, "One-dimensional electron localization in semiconductors coupled to electromagnetic cavities," Phys. Rev. B, vol. 109, no. 4, p. 045432, 2024.
- [31] D. N. Basov, A. Asenjo-Garcia, P. J. Schuck, X. Zhu, and A. Rubio, "Polariton panorama," Nanophotonics, vol. 10, no. 1, pp. 549-577,
- [32] L. A. Khalfin, "Contribution to the decay theory of a guasistationary state," Sov. Phys. JETP, vol. 6, no. 6, p. 1053, 1958.
- [33] V. P. Bykov, "Spontaneous emission from a medium with a band spectrum," Sov. J. Quantum Electron., vol. 4, no. 7, pp. 861-871,
- [34] L. Fonda, G. C. Ghirardi, and A. Rimini, "Decay theory of unstable quantum systems," Rep. Prog. Phys., vol. 41, no. 4, p. 587, 1978.
- [35] D. S. Onley and A. Kumar, "Time dependence in quantum mechanics – study of a simple decaying system," Am. J. Phys., vol. 60, no. 5, p. 432, 1992.
- [36] B. Gaveau and L. S. Schulman, "Limited quantum decay," J. Phys. A Math. Gen., vol. 28, no. 24, pp. 7359-7374, 1995.
- [37] S. Garmon, H. Nakamura, N. Hatano, and T. Petrosky, "Two-channel quantum wire with an adatom impurity: role of the van Hove singularity in the quasibound state in continuum, decay rate amplification, and the Fano effect," Phys. Rev. B, vol. 80, no. 11, p. 115318, 2009.
- [38] S. Garmon, T. Petrosky, L. Simine, and D. Segal, "Amplification of non-Markovian decay due to bound state absorption into continuum," Fortschr. Phys., vol. 61, nos. 2-3, p. 261, 2013.
- [39] S. Garmon, "Bound state influence on long-time non-exponential decay in open quantum systems," in The Rochester Conferences on Coherence and Quantum Optics and the Quantum Information and Measurement meeting, OSA, 2013.
- [40] F. Lombardo, F. Ciccarello, and G. M. Palma, "Photon localization versus population trapping in a coupled-cavity array," Phys. Rev. A, vol. 89, no. 5, p. 053826, 2014.
- [41] E. Sánchez-Burillo, D. Zueco, L. Martín-Moreno, and J. J. García-Ripoll, "Dynamical signatures of bound states in waveguide qed," Phys. Rev. A, vol. 96, no. 2, p. 023831, 2017.
- [42] A. González-Tudela, C.-L. Hung, D. E. Chang, J. I. Cirac, and H. J. Kimble, "Subwavelength vacuum lattices and atom – atom interactions in two-dimensional photonic crystals," Nat. Photonics, vol. 9, no. 5, p. 320, 2015.
- [43] J. S. Douglas, H. Habibian, C.-L. Hung, A. V. Gorshkov, H. J. Kimble, and D. E. Chang, "Quantum many-body models with cold atoms coupled to photonic crystals," Nat. Photonics, vol. 9, no. 5, p. 326, 2015.
- [44] T. Shi, Y.-H. Wu, A. González-Tudela, and J. I. Cirac, "Bound states in boson impurity models," Phys. Rev. X, vol. 6, no. 2, p. 021027, 2016.
- [45] G. Calajó, F. Ciccarello, D. Chang, and P. Rabl, "Atom-field dressed states in slow-light waveguide qed," Phys. Rev. A, vol. 93, no. 3, p. 033833, 2016.

- [46] A. González-Tudela and J. I. Cirac, "Markovian and non-Markovian dynamics of quantum emitters coupled to two-dimensional structured reservoirs," Phys. Rev. A, vol. 96, no. 4, p. 043811, 2017.
- [47] A. González-Tudela and J. I. Cirac, "Quantum emitters in two-dimensional structured reservoirs in the nonperturbative regime," Phys. Rev. Lett., vol. 119, no. 14, p. 143602, 2017.
- [48] A. González-Tudela and J. I. Cirac, "Non-Markovian quantum optics with three-dimensional state-dependent optical lattices," Quantum, vol. 2, p. 97, 2018.
- [49] A. González-Tudela and J. I. Cirac, "Exotic quantum dynamics and purely long-range coherent interactions in Dirac conelike baths," Phys. Rev. A, vol. 97, no. 4, p. 043831, 2018.
- [50] A. González-Tudela and F. Galve, "Anisotropic quantum emitter interactions in two-dimensional photonic-crystal baths," ACS Photonics, vol. 6, no. 1, p. 221, 2018.
- [51] T. Shi, Y. H. Wu, A. González-Tudela, and J. I. Cirac, "Effective many-body Hamiltonians of qubit-photon bound states," New J. Phys., vol. 20, no. 10, p. 105005, 2018.
- [52] M. Bello, G. Platero, J. I. Cirac, and A. González-Tudela, "Unconventional quantum optics in topological waveguide qed," Sci. Adv., vol. 5, no. 7, p. eaaw0297, 2019.
- [53] E. Sánchez-Burillo, C. Wan, D. Zueco, and A. González-Tudela, "Chiral quantum optics in photonic sawtooth lattices," 2019, arXiv preprint arXiv:1907.00840.
- [54] J. Román-Roche, E. Sánchez-Burillo, and D. Zueco, "Bound states in ultrastrong waveguide qed," Phys. Rev. A, vol. 102, no. 2, p. 023702,
- [55] K. Lenk and M. Eckstein, "Collective excitations of the u(1)-symmetric exciton insulator in a cavity," Phys. Rev. B, vol. 102, no. 20, p. 205129, 2020.
- [56] D. De Bernardis, M. Jeannin, J.-M. Manceau, R. Colombelli, A. Tredicucci, and I. Carusotto, "Magnetic-field-induced cavity protection for intersubband polaritons," Phys. Rev. B, vol. 106, no. 22, p. 224206, 2022.
- [57] Z. Bacciconi, G. M. Andolina, T. Chanda, G. Chiriacò, M. Schirò, and M. Dalmonte, "First-order photon condensation in magnetic cavities: a two-leg ladder model," SciPost Phys., vol. 15, no. 3, p. 113,
- [58] E. Vlasiuk, V. K. Kozin, J. Klinovaja, D. Loss, I. V. Iorsh, and I. V. Tokatly, "Cavity-induced charge transfer in periodic systems: length-gauge formalism," Phys. Rev. B, vol. 108, no. 8, p. 085410,
- [59] Y. Zhang, L. Yu, J. Q. Liang, G. Chen, S. Jia, and F. Nori, "Quantum phases in circuit qed with a superconducting qubit array," Sci. Rep., vol. 4, no. 1, p. 4083, 2014.
- [60] C. F. Lee and N. F. Johnson, "First-order superradiant phase transitions in a multiqubit cavity system," Phys. Rev. Lett., vol. 93, no. 8, p. 083001, 2004.
- [61] S. Gammelmark and K. Mølmer, "Phase transitions and heisenberg limited metrology in an Ising chain interacting with a single-mode cavity field," New J. Phys., vol. 13, no. 5, p. 053035,
- [62] J. Román-Roche, Á. Gómez-León, F. Luis, and D. Zueco, "Cavity ged materials: comparison and validation of two linear response theories at arbitrary light-matter coupling strengths," 2024, arXiv:2406.11971.
- [63] E. Cortese, L. Garziano, and S. De Liberato, "Polariton spectrum of the Dicke-Ising model," Phys. Rev. A, vol. 96, no. 5, p. 053861, 2017.

- [64] J. Rohn, M. Hörmann, C. Genes, and K. P. Schmidt, "Ising model in a light-induced quantized transverse field," Phys. Rev. Res., vol. 2, no. 2, p. 023131, 2020.
- [65] A. Schellenberger and K. P. Schmidt, "(Almost) everything is a Dicke model — mapping non-superradiant correlated light-matter systems to the exactly solvable Dicke model," SciPost Phys. Core, vol. 7, no. 3, p. 038, 2024.
- [66] A. Langheld, M. Hörmann, and K. P. Schmidt, "Quantum phase diagrams of Dicke-Ising models by a wormhole algorithm," 2024, arXiv:2409.15082 [cond-mat.str-el].
- [67] R. D. McKenzie, M. Libersky, D. M. Silevitch, and T. F. Rosenbaum, "Theory of magnon polaritons in quantum Ising materials," Phys. Rev. A, vol. 106, no. 4, p. 043716, 2022.
- [68] J. Román-Roche and D. Zueco, "Effective theory for matter in non-perturbative cavity QED," SciPost Phys. Lect. Notes, vol. 50, 2022, https://doi.org/10.21468/scipostphyslectnotes.50.
- [69] S. Sachdev, Quantum Phase Transitions, 2nd ed. New York, USA, Cambridge University Press, 2011.
- [70] P. Pfeuty, "The one-dimensional Ising model with a transverse field," Ann. Phys., vol. 57, no. 1, pp. 79-90, 1970.
- [71] A. Altland and B. D. Simons, Condensed Matter Field Theory, New York, USA, Cambridge University Press, 2010.
- [72] P. Prelovsek and I. Sega, "Quantum versus classical domain walls in the Ising chain with a transverse field," J. Phys. C: Solid State Phys., vol. 14, no. 22, pp. 3231-3246, 1981.
- [73] Y. Ashida, A. M. C. İmamoğlu, and E. Demler, "Cavity quantum electrodynamics at arbitrary light-matter coupling strengths," Phys. Rev. Lett., vol. 126, no. 15, p. 153603, 2021.
- [74] S. John and J. Wang, "Quantum electrodynamics near a photonic band gap: photon bound states and dressed atoms," Phys. Rev. Lett., vol. 64, no. 20, p. 2418, 1990.
- [75] E. Cortese, I. Carusotto, R. Colombelli, and S. De Liberato, "Strong coupling of ionizing transitions," Optica, vol. 6, no. 3, p. 354,
- [76] E. Cortese, et al., "Excitons bound by photon exchange," Nat. Phys., vol. 17, no. 1, pp. 31-35, 2020.
- [77] J. Román-Roche, Á. Gómez-León, F. Luis, and D. Zueco, "Linear response theory for cavity ged materials," 2024, arXiv:2406.11957.
- [78] P. A. Pantazopoulos, J. Feist, F. J. García-Vidal, and A. Kamra, "Unconventional magnetism mediated by spin-phonon-photon coupling," Nat. Commun., vol. 15, no. 1, p. 4000, 2024.
- [79] D. Kim, et al., "Observation of the magnonic dicke superradiant phase transition," 2024, arXiv:2401.01873 [quant-ph].
- [80] C. J. S. Martínez, F. Lindel, F. J. García-Vidal, and J. Feist, "General theory of cavity-mediated interactions between low-energy matter excitations," 2024, arXiv:2407.19478 [quant-ph], https://doi.org/10 .1063/5.0231058.
- [81] K. Kakazu and Y. S. Kim, "Quantization of electromagnetic fields in cavities and spontaneous emission," Phys. Rev. A, vol. 50, no. 2, p. 1830, 1994.
- [82] D. A. Steck, Quantum and Atom Optics, Cambridge, Cambridge University Press, 2007.
- [83] A. Stokes and A. Nazir, "Implications of gauge freedom for nonrelativistic quantum electrodynamics," Rev. Mod. Phys., vol. 94, no. 4, p. 045003, 2022.
- [84] K. Lenk, J. Li, P. Werner, and M. Eckstein, "Collective theory for an interacting solid in a single-mode cavity," 2022, arXiv:2205.05559.
- [85] G. M. Andolina, F. M. D. Pellegrino, V. Giovannetti, A. H. MacDonald, and M. Polini, "Cavity quantum electrodynamics

- of strongly correlated electron systems: a no-go theorem for photon condensation," Phys. Rev. B, vol. 100, no. 12, p. 121109, 2019.
- [86] G. M. Andolina, F. M. D. Pellegrino, V. Giovannetti, A. H. MacDonald, and M. Polini, "Theory of photon condensation in a spatially varying electromagnetic field," Phys. Rev. B, vol. 102, no. 12, p. 125137, 2020.
- [87] G. M. Andolina, F. M. D. Pellegrino, A. Mercurio, O. D. Stefano, M. Polini, and S. Savasta, "No-go theorem for photon condensation: a non-perturbative extension to first-order phase transitions," 2021, arXiv:2104.09468 [cond-mat.mes-hall].
- [88] V. Rokaj, D. M. Welakuh, M. Ruggenthaler, and A. Rubio, "Light – matter interaction in the long-wavelength limit: no ground-state without dipole self-energy," J. Phys. B: At. Mol. Opt. Phys., vol. 51, no. 3, p. 034005, 2018.
- [89] C. Schäfer, M. Ruggenthaler, V. Rokaj, and A. Rubio, "Relevance of the quadratic diamagnetic and self-polarization terms in cavity quantum electrodynamics," ACS Photonics, vol. 7, no. 4, pp. 975-990, 2020.

- [90] D. Lamberto, O. D. Stefano, S. Hughes, F. Nori, and S. Savasta, "Quantum phase transitions in many-dipole light-matter systems," 2024, arXiv:2405.10711 [quant-ph].
- [91] O. Di Stefano, et al., "Resolution of gauge ambiguities in ultrastrong-coupling cavity quantum electrodynamics," Nat. Phys., vol. 15, no. 8, pp. 803-808, 2019.
- [92] L. Garziano, A. Settineri, O. Di Stefano, S. Savasta, and F. Nori, "Gauge invariance of the dicke and hopfield models," Phys. Rev. A, vol. 102, no. 2, p. 023718, 2020.
- [93] S. Savasta, O. Di Stefano, A. Settineri, D. Zueco, S. Hughes, and F. Nori, "Gauge principle and gauge invariance in two-level systems," Phys. Rev. A, vol. 103, no. 5, p. 053703, 2021.
- [94] O. Dmytruk and M. Schiró, "Gauge fixing for strongly correlated electrons coupled to quantum light," Phys. Rev. B, vol. 103, no. 7, p. 075131, 2021.
- [95] J. Li, D. Golez, G. Mazza, A. J. Millis, A. Georges, and M. Eckstein, "Electromagnetic coupling in tight-binding models for strongly correlated light and matter," Phys. Rev. B, vol. 101, no. 20, p. 205140, 2020.